A VISCOUS - INVISCID INTERACTION FOR AERODYNAMIC AND AEROELASTIC CALCULATION

W. K. Sekar *), C. Weishäupl **), B. Laschka *)
*) Institute for Fluid Mechanics, Technische Universität München
Boltzmannstrasse 15, 85748 Garching, Germany
**) EADS Military Aircraft, MT242, 81663 Munich, Germany

Keywords: *viscous-inviscid interaction, integral boundary layer, TSD equation, Euler equations, state space equation*

Abstract

A viscous - inviscid interaction (VII) to calculate aerodynamic characteristics and its application for flutter calculation of an airfoil or a wing in turbulent flow has been developed at Institute for Fluid Mechanics (FLM) of Technische Universität München (TUM) as an alternative solution of the Navier - Stokes equations. The viscous flow will be modeled by the integral boundary layer equations and the and inviscid flow either by the transonic small disturbance (TSD) equation or by the Euler equations. The interaction between inner viscous and outer inviscid flow will be carried out through the transpiration boundary condition in the inviscid flow model.

The integral boundary layer equations will be solved by a 4th order Runge - Kutta method using additional closure equations from Drela and Giles. The treatment of the boundary layer in spanwise direction will be carried out using the strip theory approach. The TSD equation will be solved using a finite difference method with an approximate factorization algorithm. The Euler equations are solved using an upwind scheme of Roe's type employing cell centred finite volume discretization and implicit LU-SSOR time integration from Yoon and Jameson.

Furthermore this VII method will be coupled with the structural motion of an airfoil or a wing to calculate its aeroelastic response. The equation of motion involving fluid and structure will be written in a state space equation, which will be solved using a state transition matrix technique.

Calculations of the aerodynamic behaviour are performed for several airfoils and wings in transonic flow, while aeroelastic calculations aim to calculate the transonic dip. A comparison with other numerical and experimental results will be presented and shows good agreement.

Nomenclature

α_0 , α_1 = mean value and amplitude of angle of attack
ρ = density
τ = shear stress, computational time
$\delta^* = \int_0^\infty \left(1-\frac{\rho U}{\rho_e U_e}\right) dz$ = displacement thickness
$\delta^{**} = \int_0^\infty \left(1-\frac{\rho}{\rho_e}\right)\frac{U}{U_e} dz$ = density thickness
$\theta = \int_0^\infty \left(1-\frac{U}{U_e}\right)\frac{\rho U}{\rho_e U_e} dz$ = momentum thickness
$\theta^* = \int_0^\infty \left(1-\frac{U^2}{U_e^2}\right)\frac{\rho U}{\rho_e U_e} dz$ = kinetic energy thickness
γ = ratio of heat capacity
ξ,, η, ζ = computational coordinate directions
ϕ = potential of disturbance velocity
ω_h , ω_α = natural frequency in heave and pitch
b = semi chord
$C_f = \frac{2\tau_w}{\rho_e U_e^2}$ = skin friction coefficient
$C_d = \frac{1}{\rho_e U_e^3}\int_0^\infty \tau \frac{dU}{dz} dz$ = dissipation coefficient
C_l = lift coefficient
C_p = pressure coefficient
c, c_r = chord, root chord length
e = total energy
H = δ^*/θ = displacement shape factor
H_k = kinematic shape factor
H^* = θ^*/θ = energy shape factor
H^{**} = δ^{**}/θ = density shape factor
k = $\omega c/U_\infty$,reduced frequency
m = mass
M, Re = Mach and Reynolds number
s = semi span
t = time

u, v, w = velocity components in x, y, z
U = tangential velocity component
V^* = flutter speed index
x, y, z = Cartesian coordinate directions
x_p = pitching axis

Subscripts

e = edge of boundary layer
le , te = leading and trailing edge
t = time derivative
∞ = undisturbed flow condition
ξ , η, ζ = derivatives w.r.t. computational coordinates
x , y, z = derivatives w.r.t. Cartesian coordinates

Superscripts

+ , - = upper and lower surface
n = time level

1. Introduction

Nowadays, the use of flow solver based on the Navier-Stokes equations is often suggested in the design phase of a new aircraft in order to know its aerodynamic characteristics accurately [1]. However this is to be expensive and time consumptive for a daily application, especially when involving parametric studies with many design variables. This situation is more crucial for aeroelastic calculations such as flutter calculation with coupling between the structural dynamics and aerodynamic forces. There is a need for comprehensive calculation of unsteady aerodynamic forces.

Another approach to calculate the flow with its viscous influence, which is called viscous – inviscid interaction (VII) method, seems to be more economical and suitable for industry application [2]. In this approach the flow field is divided into a thin viscous flow field near the body surface covered by an inviscid flow field, which interact vice versa.

In the present analysis the viscous flow is modeled by the integral boundary layer equations and the inviscid flow by either the transonic small disturbance (TSD) equation or the Euler equations. The direct interaction between the viscous and inviscid flow model is implemented using the transpiration boundary condition in the inviscid model.

This viscous – inviscid interaction method then is coupled with the structural dynamics of the airfoil or wing to calculate its aeroelastic response. The aero-structure coupling is carried out using the state – space equation which will be solved using a state transition matrix technique.

2. Viscous Aerodynamic Model

2.1. The integral boundary layer equations

The integral momentum boundary layer and the kinetic energy shape parameter equations from Drela and Giles [2] will be used as viscous model to calculate the boundary layer parameter.

These equations can be written as follows [2]:

$$\frac{d\theta}{dx} = \frac{C_f}{2} - \left(H + 2 - M_e^2\right)\frac{\theta}{U_e}\frac{dU_e}{dx} \tag{1}$$

$$\frac{dH^*}{dx} = \frac{1}{\theta}\left(2C_d - \frac{1}{2}C_f\right) - \left(\frac{2H^{**}}{H^*} + 1 - H\right)\frac{H^*}{U_e}\frac{dU_e}{dx} \tag{2}$$

These equations will be closed using several closure equations such as [2]:

$$C_f = C_f(H_k,\theta) \qquad C_d = C_d(H_k,H^*,\theta)$$
$$H = H(H_k) \quad H^* = H^*(H_k) \quad H^{**} = H^{**}(H_k) \tag{3}$$

and will be solved using a 4th order Runge - Kutta method with unknowns H^* and θ and inputs from the inviscid model: velocity U_e and Mach number M_e. The turbulent boundary layer values calculated using power 1/7 law [3] will be used as initial values to start the integration.

For the boundary layer calculation around a wing the strip theory is used, i.e. the boundary layer along spanwise direction is assumed to be two dimensional.

3. Inviscid Aerodynamic Models

3.1. TSD equation

The TSD equation can be written as: [4]

$$\frac{\partial f_0}{\partial t} + \frac{\partial f_1}{\partial x} + \frac{\partial f_2}{\partial y} + \frac{\partial f_3}{\partial z} = 0 \tag{4}$$

where the fluxes are defined as:

$$f_0 = -\left(A\phi_t + B\phi_x\right) \tag{5a}$$
$$f_1 = E\phi_x + F\phi_x^2 + G\phi_y^2 \tag{5b}$$
$$f_2 = \phi_y + H\phi_x\phi_y \tag{5c}$$
$$f_3 = \phi_z \tag{5d}$$

The coefficients A, B, E, F, G and H are:

$$A = M_\infty^2 \qquad B = 2M_\infty^2 \qquad E = 1 - M_\infty^2$$
$$F = -\frac{1}{2}(\gamma+1)M_\infty^2 \qquad G = \frac{1}{2}(\gamma-3)M_\infty^2 \qquad H = -(\gamma-1)M_\infty^2 \tag{6}$$

Equation (4) can be written simply as:

$$\bar{R}\left(\phi^{n+1}\right) = 0 \tag{7}$$

where $\bar{R}$ is a differential operator.

3.1.1. Solution of the TSD equation

The potential of the disturbance velocity ϕ at a specified time level $n+1$ will be stated as:

$$\phi^{n+1} = \phi^{*} + \Delta\phi \tag{8}$$

with ϕ* is an assumed value of ϕ^{n+1}.

By applying the 1st order Taylor series approximation in the equation (7), one obtains:

$$\left(\frac{\partial \bar{R}}{\partial \phi}\right)_{\phi=\phi^{*}} \Delta\phi = -\bar{R}(\phi^{*}) \tag{9}$$

The LHS of Eq.(9) is approximately factorized into a product of independent operators L_ξ , L_η and L_ζ as [4]:

$$L_\xi L_\eta L_\zeta \ \Delta\phi = R(\phi^{*}, \phi^{n}, \phi^{n-1}, \phi^{n-2}) \tag{10}$$

with:

$$L_\xi = 1 + \frac{3B}{4A}\Delta t \xi_x \frac{\partial}{\partial \xi} - \frac{\Delta t^2}{2A}\xi_x \frac{\partial}{\partial \xi}\frac{\partial}{\partial \xi}$$
$$\left[E\xi_x + 2F\xi_x{}^2\phi^{*}_{\xi} + (2G+H)\xi_y\left(\xi_y\phi^{*}_{\xi} + \phi^{*}_{\eta}\right) + \frac{\xi_y^2}{\xi_x} + H\xi_y^2\phi^{*}_{\xi}\right]$$

$$L_\eta = 1 - \frac{\Delta t^2}{2A}\frac{\partial}{\partial \eta}\frac{\partial}{\partial \eta}\left(1 + H\phi^{*}_{\xi}\xi_x\right)$$

$$L_\zeta = 1 - \frac{\Delta t^2}{2A}\frac{\partial}{\partial \zeta}\frac{\partial}{\partial \zeta}$$

$$R(\phi^{*}, \phi^{n}, \phi^{n-1}, \phi^{n-2}) = -\frac{1}{2}\left(2\phi^{*} - 5\phi^{n} + 4\phi^{n-1} - \phi^{n-2}\right) -$$
$$\frac{B}{4A}\Delta t\xi_x\left(3\phi^{*}_{x} - 4\phi^{n}_{x} + \phi^{n-1}_{x}\right) +$$
$$\frac{(\Delta t)^2}{2A}\xi_x\frac{\partial}{\partial \xi}\left(\begin{array}{l} E\xi_x\phi^{*}_{\xi} + F\xi_x{}^2(\phi^{*}_{\xi})^2 + G(\xi_y\phi^{*}_{\xi} + \phi^{*}_{\eta})^2 + \\ \frac{\xi_y}{\xi_x}\left(\xi_y\phi^{*}_{\xi} + \phi^{*}_{\eta}\right)\left(1 + H\xi_x\phi^{*}_{\xi}\right) \end{array}\right) +$$
$$\frac{(\Delta t)^2}{2A}\frac{\partial}{\partial \eta}\left[\left(\xi_y\phi^{*}_{\xi} + \phi^{*}_{\eta}\right)\left(1 + H\xi_x\phi^{*}_{\xi}\right)\right] + \frac{(\Delta t)^2}{2A}\frac{\partial}{\partial \zeta}\phi^{*}_{\xi} \tag{11}$$

The time derivative is discretized using 2nd order backward difference and the space derivatives are dicretized using 1st order backward or 2nd order central difference for local supersonic or subsonic flow, respectively. The computational coordinates are simply related to the physical coordinates as follows:

$$\xi = \frac{x - x_{le}(y)}{c(y)}, \quad \eta = y/s, \quad \zeta = z/c_r \tag{12}$$

The solution procedure of Eq. (10) involves three sweeping processes in the stream ξ, span η and vertical ζ direction, as follows:

ξ sweep: $L_\xi \Delta\phi^{\xi} = R(\phi^{*}, \phi^{n}, \phi^{n-1}, \phi^{n-2})$ (13)

where $\Delta\phi^{\xi} = L_\eta L_\zeta \ \Delta\phi$

η sweep: $L_\eta \Delta\phi^{\eta} = \Delta\phi^{\xi}$ (14)

where $\Delta\phi^{\eta} = L_\zeta \ \Delta\phi$

ζ sweep: $L_\zeta \ \Delta\phi = \Delta\phi^{\eta}$ (15)

The solution ϕ^{n+1} can be calculated using eq. (8). This sweeping procedure must be carried out until a converged value is achieved.

An entropy correction introduced by Fuglsang [5] due to the discontinuity of pressure across a shock wave is also implemented in this TSD equation and its influence will be used to update the velocity field behind a shock [4].

3.1.2. Boundary Conditions

The TSD equation must be solved subjected to the tangential boundary condition on the surface as follows:

$$\phi_z^{\pm} = f_x^{\pm} + \delta_x^{*\pm} \tag{16}$$

where f is the ordinate of the surface and δ^{*} is the displacement thickness due to boundary layer on the surface.

3.2. The Euler Equations

The Euler equations can be written in computational coordinates as follows [6]:

$$\frac{\partial\{Q\}}{\partial\tau} + \frac{\partial\{F\}}{\partial\xi} + \frac{\partial\{G\}}{\partial\eta} + \frac{\partial\{H\}}{\partial\varsigma} = 0 \tag{17}$$

where the vector $\{Q\}$ and fluxes $\{F\},\{G\},\{H\}$ are: $\{Q\} = J\{q\}$

$$\begin{aligned} \{F\} &= J\xi_t\{q\} + J\xi_x\{f\} + J\xi_y\{g\} + J\xi_z\{h\} \\ \{G\} &= J\eta_t\{q\} + J\eta_x\{f\} + J\eta_y\{g\} + J\eta_z\{h\} \\ \{H\} &= J\varsigma_t\{q\} + J\varsigma_x\{f\} + J\varsigma_y\{g\} + J\varsigma_z\{h\} \end{aligned} \tag{18}$$

The vector $\{q\}$ and fluxes $\{f\},\{g\},\{h\}$ are:

$$\{q\} = [\rho, \rho u, \rho v, \rho w, e]^T \tag{19a}$$
$$\{f\} = [\rho u, \rho uu + p, \rho uv, \rho uw, (e+p)u]^T \tag{19b}$$
$$\{g\} = [\rho v, \rho vu, \rho vv + p, \rho vw, (e+p)v]^T \tag{19c}$$
$$\{h\} = [\rho w, \rho wu, \rho wv, \rho ww + p, (e+p)w]^T \tag{19d}$$

and the Jacobian is:

$$J = \frac{\partial(x,y,z,t)}{\partial(\xi,\eta,\varsigma,\tau)} = x_\xi\left(y_\eta z_\varsigma - z_\eta y_\varsigma\right) - y_\xi\left(x_\eta z_\varsigma - z_\eta x_\varsigma\right) + z_\xi\left(x_\eta y_\varsigma - y_\eta x_\varsigma\right) \tag{20}$$

To close the problem the pressure relation will be chosen as the closure equation:

$$p = (\gamma - 1)\left[e - \frac{\rho}{2}\left(u^2 + v^2 + w^2\right)\right] \tag{21}$$

3.2.1. Solution of the Euler Equations

To solve the Euler equations (17) numerically the finite volume method will be used. These equations will be discretized in space as:

$$\frac{\partial \{Q\}_{k,l,m}}{\partial \tau} = -R_{k,l,m} \quad (22)$$

with R is given by:

$$R_{k,l,m} = \left|\{F\}_{k+1/2,l,m} - \{F\}_{k-1/2,l,m}\right| + \left|\{G\}_{k,l+1/2,m} - \{G\}_{k,l-1/2,m}\right| + \left[\{H\}_{k,l,m+1/2} - \{H\}_{k,l,m-1/2}\right] \quad (23)$$

The indices k, l, m define the cells number in the computational coordinates ξ, η, ζ respectively. Fig. 1. shows the scheme of the discretization in ξ direction.

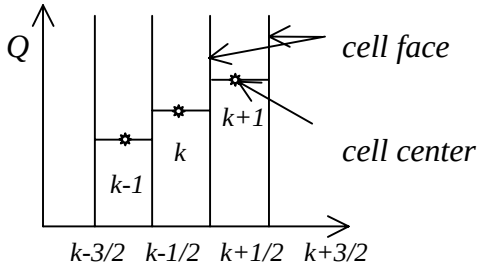

Fig. 1. Scheme of the discretization

The Riemann Problem at the cell face will be approximated using a flux difference splitting technique which is purposed by Roe [7] The time integration of the Eq. (22) will be carried out by implicit LU-SSOR (Lower Upper Symmetric Successive Over Relaxation) which is introduced by Yoon and Jameson [8].

The equation (22) will be discretized in time as:

$$\Delta Q = Q^{n+1} - Q^n = -R^{n+1}\Delta\tau \quad (24)$$

Performing the Taylor approximation in R as:

$$R^{n+1} = R^n + \left.\frac{\partial R}{\partial Q}\right|_n \Delta Q \quad (25)$$

Eq.(24) becomes to:

$$\left(I + \Delta\tau \left.\frac{\partial R}{\partial Q}\right|_n\right)\Delta Q = -\Delta\tau R^n \quad (26)$$

The LHS term of Eq. (26) will be approximated as a summation of three matrices D (Diagonal), U (Upper) and L (Lower) as follows:

$$\left[D + U + L\right]\Delta Q = -R^n_{k,l,m} \quad (27)$$

which is then further approximated into:

$$\left[D + L\right]\left[D^{-1}(D + U)\right]\Delta Q = -R^n_{k,l,m} \quad (28)$$

The expression of the matrices D, L and U can be found in Ref. [8].

The solution of Eq. (28) is involving two steps sweeping:

1st step: $\left[D + L\right]\Delta Q^* = -R^n_{k,l,m}$ (29)

2nd step:

$$\left[D^{-1}(D + U)\right]\Delta Q = \Delta Q^*$$

$$\left[D + U\right]\Delta Q = D\Delta Q^* \quad (30)$$

The value of vector Q at the new time step is:

$$Q^{n+1} = Q^n + \Delta Q \quad (31)$$

This procedure will be carried out until convergence.

For the unsteady problem, a pseudo time step is used to obtain the solution with respect to the new position of the body, but the sweeping procedure remains the same [8].

3.2.2. Boundary Condition

The Euler equations must be solved subjected to the tangential boundary condition as follows:

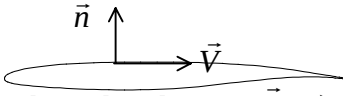

without boundary layer : $\vec{V} \bullet \vec{n} = 0$ (32a)

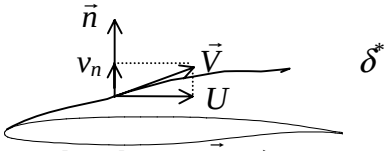

with boundary layer: $\vec{V} \bullet \vec{n} = v_n = U\dfrac{d\delta^*}{dx}$ (32b)

Fig. 2. Tangential boundary condition

4. Direct Viscous – Inviscid Interaction

The direct viscous-inviscid interaction can be described by a functional diagram, Fig. 3. The inviscid model generates the velocity distribution U_e, which will be used as input for viscous model. The output displacement thickness δ^* from the viscous model will be back used to update the tangential boundary condition of the inviscid model. This process will be repeated until convergence.

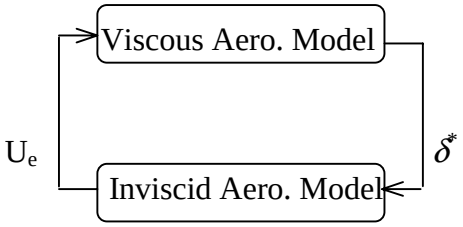

Fig. 3. Direct viscous-inviscid interaction

5. Fluid – Structure Coupling

5.1. Equation of Motion

The equation of motion of an aeroelastic system is written in term of generalized displacement $\{q\}$. For this purpose the physical displacement $\{z\}$ is assumed to be [9]:

$$\{z\} = [\Phi]\{q\} \tag{33}$$

where [Φ] are the vibration mode shapes.
Then the equation of motion can be written as:

$$[M]\left\{\ddot{q}\right\} + [C]\left\{\dot{q}\right\} + [K]\{q\} = \{Q\} \tag{34}$$

with [M], [C], [K] and {Q} are the generalized mass, damping, stiffness and aerodynamic forces matrix respectively.
The relations between generalized mass, damping and stiffness can be written as [9]:

$$[K] = [\omega_n^2 M] \quad [C] = [2\varsigma][K]^{1/2}[M]^{1/2} \tag{35}$$

with ω_n and ζ are natural frequency and modal damping coefficient respectively.

5.2. Solution of the Equation of Motion

The equation of motion (34) can be formulated as a state space equation as follows:

$$\begin{Bmatrix}\dot{q}\\ \ddot{q}\end{Bmatrix} = \begin{bmatrix}0 & [I]\\ -[M]^{-1}[K] & -[M]^{-1}[C]\end{bmatrix}\begin{Bmatrix}q\\ \dot{q}\end{Bmatrix} + \begin{bmatrix}0 & 0\\ 0 & [M]^{-1}\end{bmatrix}\begin{Bmatrix}0\\ Q\end{Bmatrix} \tag{36}$$

which can be recasted as follows:

$$\left\{\dot{X}\right\} = [A]\{X\} + [B]\{u\} \tag{37}$$

Solution of the state space equation (37) at the next time step $n+1$ is:

$$\{X^{n+1}\} = L_h + L_{nh} \tag{38}$$

with the homogeneous solution:

$$L_h = \exp[A\Delta\tau]\{X(n\Delta\tau)\} = [\psi_h]\{X^n\} \tag{39}$$

where the State Transition Matrix [ψ_h] is [10]:

$$\psi_{h11} = e^{-[\varsigma\omega_n]\Delta\tau}\left\{\begin{matrix}\cos[\omega_n(1-\varsigma^2)^{1/2}\Delta\tau] + \\ \varsigma(1-\varsigma^2)^{-1/2}\sin[\omega_n(1-\varsigma^2)^{1/2}\Delta\tau]\end{matrix}\right\}$$
$$\psi_{h12} = e^{-[\varsigma\omega_n]\Delta\tau}\omega_n^{-1}(1-\varsigma^2)^{-1/2}\sin[\omega_n(1-\varsigma^2)^{1/2}\Delta\tau]$$
$$\psi_{h21} = -e^{-[\varsigma\omega_n]\Delta\tau}\omega_n(1-\varsigma^2)^{-1/2}\sin[\omega_n(1-\varsigma^2)^{1/2}\Delta\tau]$$
$$\psi_{h22} = e^{-[\varsigma\omega_n]\Delta\tau}\left\{\begin{matrix}\cos[\omega_n(1-\varsigma^2)^{1/2}\Delta\tau] - \\ \varsigma(1-\varsigma^2)^{-1/2}\sin[\omega_n(1-\varsigma^2)^{1/2}\Delta\tau]\end{matrix}\right\} \tag{40}$$

The non homogeneous solution is as follows:

$$L_{nh} = \int_{n\Delta\tau}^{(n+1)\Delta\tau}\exp[A((n+1)\Delta\tau - \tau^*)][B]\{u(\tau^*)\}d\tau^* \tag{41}$$
$$\cong [\psi_{nh}][B]\left(\{u^{n+1}\} + \{u^n\}\right)/2$$

with the State Transition Matrix [ψ_{nh}] :

$$[\psi_{nh}] = [A]^{-1}\exp[A\tau^*]_0^{\Delta\tau} = \begin{bmatrix}-2\varsigma/\omega_n & -\omega_n^{-2}\\ 1 & 0\end{bmatrix}[\psi_h]_0^{\Delta\tau} \tag{42}$$

which can be formulated as follows:

$$\psi_{nh11} = e^{-[\varsigma\omega_n]\Delta\tau}\left\{\begin{matrix}\frac{-2\varsigma}{\omega_n}\cos[\omega_n(1-\varsigma^2)^{1/2}\Delta\tau] + \\ \left(\frac{1-2\varsigma^2}{\omega_n(1-\varsigma^2)^{1/2}}\right)\sin[\omega_n(1-\varsigma^2)^{1/2}\Delta\tau]\end{matrix}\right\} + \frac{2\varsigma}{\omega_n}$$
$$\psi_{nh12} = -e^{-[\varsigma\omega_n]\Delta\tau}\left\{\begin{matrix}\frac{\varsigma}{\omega_n^2(1-\varsigma^2)^{1/2}}\sin[\omega_n(1-\varsigma^2)^{1/2}\Delta\tau] + \\ \frac{1}{\omega_n^2}\cos[\omega_n(1-\varsigma^2)^{1/2}\Delta\tau]\end{matrix}\right\} + \frac{1}{\omega_n}$$
$$\psi_{nh21} = e^{-[\varsigma\omega_n]\Delta\tau}\left\{\begin{matrix}\frac{\varsigma}{(1-\varsigma^2)^{1/2}}\sin[\omega_n(1-\varsigma^2)^{1/2}\Delta\tau] + \\ \cos[\omega_n(1-\varsigma^2)^{1/2}\Delta\tau]\end{matrix}\right\} - 1 = \psi_{h11} - 1$$
$$\psi_{nh22} = e^{-[\varsigma\omega_n]\Delta\tau}\omega_n^{-1}(1-\varsigma^2)^{-1/2}\sin[\omega_n(1-\varsigma^2)^{1/2}\Delta\tau] = \psi_{h12} \tag{43}$$

The aerodynamic vector {u} for the next time step is assumed as a linear function from previous time steps [11]:

$$\{u^{n+1}\} \cong \{u^n\} + \left[\{u^n\} - \{u^{n-1}\}\right] \tag{44}$$

The non homogeneous solution now can be written in the following expression:

$$L_{nh} = [\psi_{nh}][B]\left(\{3u^n\} - \{u^{n-1}\}\right)/2 \tag{45}$$

Finally the response of the system for the next time step can be calculated as follows:

$$\{X^{n+1}\} = [\psi_h]\{X^n\} + [\psi_{nh}][B]\left(\{3u^n\} - \{u^{n-1}\}\right)/2 \tag{46}$$

5.3. Boundary Conditions

The coupling between structural response and aerodynamic forces occurs in the boundary condition. Using the inviscid TSD equation, the tangential boundary condition can be written as:

$$\phi_z^{\pm} = f_{x\,R}^{\pm}|_{St} + \left[f_x^{\pm} + f_t^{\pm}\right]_F|_{Ust} + \delta_x^{*\pm} \tag{47}$$

where f and δ^* are the ordinate of the surface and the displacement thickness respectively.
The first term is the steady rigid body term and the second term is the unsteady flexible body term due to the vibration modes as follows:

$$\left[f_x^{\pm} + f_t^{\pm}\right]_F|_{Ust} = [\Phi_x]\{q\} + \frac{1}{U_\infty}[\Phi]\left\{\dot{q}\right\} \tag{48}$$

where $[\Phi_x]$ is the slope of vibration modes.

6. Results

6. 1. Aerodynamic Results

An unsteady pitching motion case of an NACA 0012 airfoil with the following data: M=0.755, Re=5.5E+06, α_0=0.016°, α_1=2.51°, k=0.1628, x_p=0.25c is calculated using the TSD equation as inviscid model. The time histories of lift and moment coefficient is depicted in Fig.

4. The experimental results from Landon [12] and the Navier-Stokes solutions using the Baldwin-Lomax turbulence model (NS-BL) from Cvrlje [13] are used for comparison. The present method shows an excellent agreement with the Navier-Stokes solutions especially for the lift coefficient.

As the second case, a pitching motion of a NACA 64A010 airfoil with the following data: M=0.796, Re=1.2E+07, α_0=0, α_1=1.02, k=0.404, x_p=0.25c will be simulated using the TSD equation as inviscid model. Fig. 5 shows comparison of the time histories of lift and moment coefficient between experimental results from Davis [14] and numerical results using the present method. A good agreement with experiment can be observed for this case. The influence of boundary layer in the inviscid results seems to be small.

As the third case, an unsteady pitching motion case of a NLR 7301 airfoil is calculated using the TSD equation as the inviscid model. The flow and motion data are: M=0.7, Re=2.14E+06, α_0=2.0, α_1=0.5, k=0.384, x_p=0.4c. Fig. 6. shows the zero and first harmonic of the pressure distribution. The result is compared with the experimental result from Zwaan [15] and the steady solution obtained with the FLM Navier-Stokes Code from Institut of Fluid Mechanics Technical Universität München using the Baldwin-Lomax turbulence model (NS-BL). The shock position from Navier-Stokes solution seems to be too early compared to the VII result. The present results have good agreement with the experimental results.

For three dimensional case, the steady cases CT5 and CT9 of the LANN Wing (see AGARD [16]) with the following parameters:

CT5: M=0.82, Re=7.34E+06, α_0=0.6

CT9: M=0.82, Re=7.17E+06, α_0=2.2

are simulated using Euler equations as inviscid model (FLMEu Code). The Reynolds number is based on the root chord.

Figures 7 and 8 show the steady pressure distribution for both cases along three spanwise stations η = y/s = 0.20, 0.475 and 0.825.

Results from the FLM Navier-Stokes Code using the Spalart – Almaras turbulence model (NS-SA) and from experiment conducted by Zwaan [16] are used for comparison. The influence of the boundary layer for these cases can not be neglected, which is showed by the different shock position calculated with and without boundary layer. At lower angle of attack (CT5) there is a good agreement between VII, Navier-Stokes and experimental results, but for higher angle of attack (CT9) there is a major difference in the shock position at outer section of the wing. The shock position from Navier-Stokes result seems to be too early compared to the VII and experimental results.

6. 2. Aeroelastic Results

6. 2. 1. Isogai Model

The transonic dip of the Isogais 2D model will be simulated using inviscid aerodynamic model in order to validate the aeroelastic routine. The structural data of this model are as follows [17]:

r_α = 1.865, x_α = 1.8, a = -2, ω_h = 100 s^{-1},

ω_α = 100 s^{-1}, $\mu = m/(\pi\rho_\infty b^2)$ = 60

where r_α , x_α , μ and a are radius of gyration, static unbalance, mass ratio and elastic axis position, respectively. The airfoil NACA 64A010 is used with zero steady angle of attack. From modal analysis, the vibration mode shapes and the natural frequencies are found to be:

$$[\Phi]=\begin{bmatrix}1.8655 & -1.8655\\ 1 & 1\end{bmatrix} \qquad \left(\frac{\omega}{\omega_\alpha}\right)_1 = 0.7134, \quad \left(\frac{\omega}{\omega_\alpha}\right)_2 = 5.3376$$

$$[M]=\begin{bmatrix}13.6757 & 0\\ 0 & 0.2443\end{bmatrix} \qquad [K]=\begin{bmatrix}6.96 & 0\\ 0 & 6.96\end{bmatrix}$$

The TSD equation is used to represent the inviscid model at the present analysis. The time step for flutter calculation is $\Delta\tau$ = 0.09786 which corresponds to the physical time Δt = 9.786E-04 second. The initial disturbance is:

$$\{X_0\}=\left[q_1, \dot{q}_1, q_2, \dot{q}_2\right]^T = [0,0.01,0,0.01]^T$$

The diagram of flutter speed index $V^*=V_f/(b\omega_\alpha\sqrt{\mu})$ versus Mach number is presented in Fig. 9. The results using TSD equation from Isogai [17], using Euler equations from Alonso and Jameson [18] and using linearized potential equation Doublet Lattice Method (DLM) [19] are used as comparison data.

The calculated flutter speed index shows a dip at M=0.85 with V^*=0.53. All methods show good agreement in predicting this dip except the

DLM, which did not show the appearance of this dip. The flutter speed index increases after the dip drastically. The present method shows the rapid changing in flutter speed occurred at Mach number 0.87, which seems to be earlier compared to the result from Alonso and Jameson. Isogai did not report the flutter condition at the range from M=0.85 to M=0.9.

6.2.2. DLR Model

The transonic dip of the DLRs model is simulated using inviscid and VII aerodynamic model. The structural data of the DLRs model are:

$$r_\alpha = 0.197,\ x_\alpha = 0.0484,\ a = 0.25,$$
$$\omega_h = 206.6\ s^{-1},\ \omega_\alpha = 271.9\ s^{-1},\ \mu = 299.5$$

which are taken from the 2nd campaign in the report from Schewe et. al. [20] neglecting the modal damping coefficients.
From modal analysis, the vibration mode shapes and the natural frequencies are found to be:

$$[\Phi] = \begin{bmatrix} 0.6851 & -0.0981 \\ 1 & 1 \end{bmatrix} \qquad \left(\frac{\omega}{\omega_\alpha}\right)_1 = 0.7343, \quad \left(\frac{\omega}{\omega_\alpha}\right)_2 = 1.0675$$

$$[M] = \begin{bmatrix} 0.5745 & 0 \\ 0 & 0.0389 \end{bmatrix} \qquad [K] = \begin{bmatrix} 0.3098 & 0 \\ 0 & 0.0443 \end{bmatrix}$$

The airfoil NLR 7310 is used with 1.25 degree steady angle of attack (uncorrected). The present calculation uses lower angle of attack, i.e. –0.5 degree, in order to obtain comparable lift coefficient with experimental result.
The steady lift coefficient for various Mach number can be seen in Fig. 10. From M=0.5 up to M=0.75 the lift coefficient obtained from the numerical simulation increases monotonic reaching its maximum value, at the other side the experimental results are almost constant in this range of Mach number. A possible explanation is that the angle of attack has been changed during the experiment. The aerodynamic loads at the rear part of the airfoil induces a pitching motion with nose down direction because of the elasticity of the model.

The diagram of flutter speed index versus Mach number is presented in Fig. 11. The time step for this calculation is $\Delta\tau$=0.0327 which corresponds to Δt=1.203E-04 s. The initial disturbances are the same as in the previous case for the Isogai model.

The calculated flutter speed index shows the transonic dip at M=0.8125, with V^* = 0.152 and 0.164 for inviscid and viscid - inviscid simulation, respectively. The experiment shows the dip at around M=0.77.

6.2.3. AGARD Wing 445.6

The geometry of the AGARD wing 445.6 and its airfoil NACA 65A004 is depicted in Fig. 12. The structural data of this wing can be obtained in Ref. [21]. Only the first two normalized vibration mode shapes (bending: ω_1=9.6 Hz and torsion: ω_2=38.2 Hz) have been used for the flutter calculation purpose. The TSD equation is used as inviscid model.

The diagram of flutter speed index versus Mach number can be seen in Fig. 13. The present result shows good agreement comparing with the result from Lee-Rausch and Batina using Euler and Navier - Stokes CFL3D Code [22, 23] and experiment from Yates [21].

7. Conclusion

A viscous-inviscid interaction method using two inviscid models - the TSD equation and the Euler equations - and its application for aeroelastic calculations has been presented. Results are showed for several airfoils and wings. The inclusion of the boundary layer can improve the aerodynamic results of the inviscid model significantly, but for the presented cases only a little improvement in the aeroelastic results is observed.

Acknowledgement

The authors thank A. Pechloff from Institute for Fluid Mechanics of the Technische Universität München for his Navier-Stokes results of NLR 7301 and LANN Wing.

References

[1] A. Jameson and J. C. Vassberg, 'Computational Fluid Dynamics for Aerodynamic Design: Its Current and Future Impact', AIAA Paper 2001-0538, 2001
[2] M. Drela and M. B. Giles; 'Viscous - Inviscid Analysis of Transonic and Low Reynolds Number Airfoils'; AIAA Journal, Vol. 25, No. 10, Oct. 1987
[3] H. Schlichting; 'Boundary Layer Theory' ; Mac Graw Hill, New York, 1960

[4] J. T. Batina, 'Efficient Algorithm for Solution of the Transonic Small Disturbance Equation'; Journal of Aircraft, Vol. 25, No.7, 1987
[5] D. F. Fuglsang and M. H. Williams, 'Non Isentropic Unsteady Transonic Small Disturbance Theory'; AIAA Paper 85-0800, 1985
[6] Hoffman, K.A., 'CFD for Engineers', University of Texas at Austin, 1989
[7] P. L. Roe, 'Appoximate Riemann Solver, Parameter Vector and Difference Schemes', Journal of Computational Physics, 43, 1981
[8] S. Yoon and A. Jameson, 'A Multigrid LU-SSOR Scheme for Approximate Newton Iteration Applied to the Euler equations', NASA CR 17954, 1986
[9] C. J. Borland and D. P. Rizzetta, 'Nonlinear Transonic Flutter Analysis', AIAA Journal, Vol.20, Nov. 1982, pp. 1606-1615
[10] R. E. Skelton, 'Dynamic Systems Control: Linear Systems Analysis and Synthesis', John Wiley and Son, New York, 1988
[11] J. W. Edwards, R. M. Bennet, W. Whitlow, D. A. Seidel, 'Time Marching Transonic Flutter Solutions Including Angle of Attack Effects ', Journal of Aircraft Vol. 20 No. 11, 1983
[12] Landon, 'NACA 0012 Oscillatory and Pitching Oscillaion', in AGARD Report no. 702, Copendium of Unsteady Aerodynamic Measurements, London, August 1982
[13] T. Cvrlje, 'Instationäre Aerodynamik des Separationsvorgangs zwischen Träger und Orbiter', Dissertation, Technische Universität München, Germany, 2001.
[14] S. S. Davis, 'NACA 64A010 (NASA Ames Model) Oscillatory Pitching', in Compendium of Unsteady Aerodynamic Measurements, AGARD Report no. 702, London, August 1982
[15] R. J. Zwaan, 'NLR 7301 Supercritical Airfoil Oscillatory Pitching and Oscillating Flap', in AGARD Report no. 702, Compendium of Unsteady Aerodynamic Measurements, London, August 1982
[16] R. J. Zwaan, 'LANN Wing, Pitching Oscillation', in AGARD Report no. 702, Compendium of Unsteady Aerodynamic Measurements (Addendum) , London, August 1982
[17] K. Isogai, 'Transonic Dip Mechanism of Flutter of a Sweptback Wing : Part II ', AIAA Journal Vol. 19 No. 9., 1981
[18] J. J. Alonso and A. Jameson, 'Fully Implicit Time Marching Aeroelastic Solutions', AIAA Paper 94-0056, 1994
[19] Albano, E. and. Rodden, W.P., ,A Doublet Lattice Method for Calculating Lift Distributions on Oscillating Surfaces in Subsonic Flows', AIAA Journal, Vol. 7. Feb.1969, pp. 279-285
[20] G. Schewe, A. Knipfer, H. Mai, and G. Dietz, 'Experimental and Numerical Investigation of Nonlinear Effects in Transonic Flutter', DLR IB 232-2002 J 01, DLR Institut of Aeroelasticity, Göttingen, 2002
[21] E. C. Yates Jr.; 'AGARD Standard Aeroelastic Configurations for Dynamic Response', AGARD R-765
[22] E. M. Lee-Rausch and J. T. Batina, 'Wing Flutter Boundary Prediction Using Unsteady Euler Method', AIAA Paper 93-1422-CP, 1993
[23] E. M. Lee-Rausch and J. T. Batina, 'Calculation of AGARD Wing 445.6 Flutter using Navier-Stokes Aerodynamics', AIAA Paper No. 93-3476, AIAA 11th Aplied Aerodynamics Conference, Monterey, California, USA, 9-11 August 1993

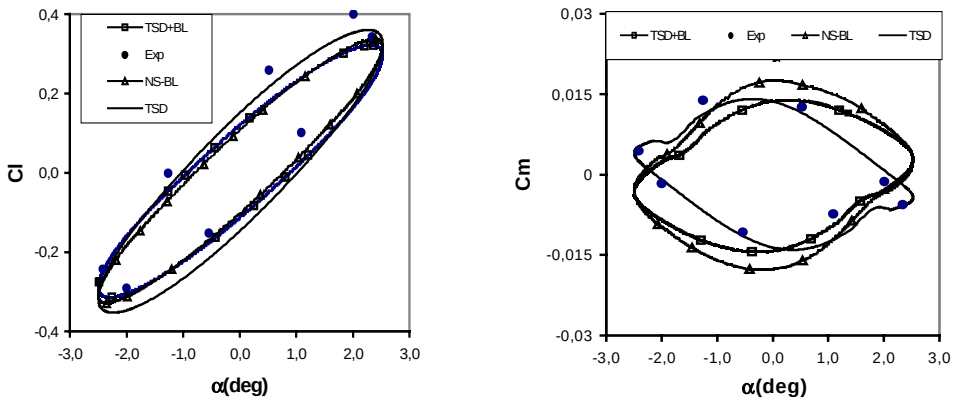

(a) Lift coefficient (b) Moment coefficient

Fig. 4. Time histories of lift and moment coefficient of a NACA 0012 airfoil
M=0.755, Re=5.5E+06, α_0=0.016, α_1=2.51, k=0.1628, x_p=0.25c

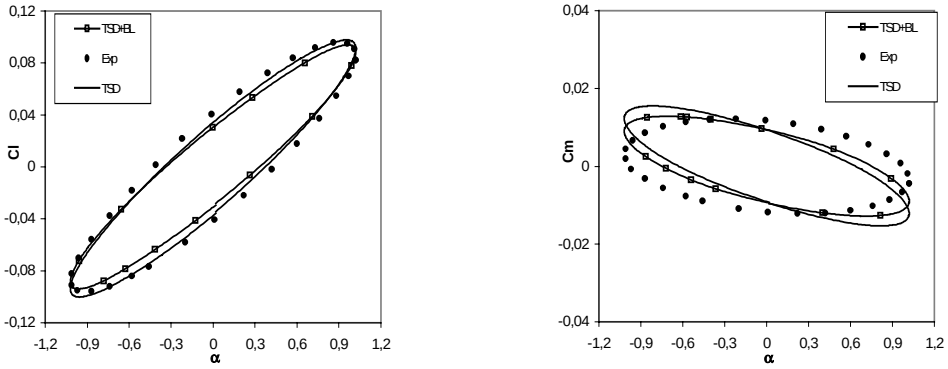

(a) Lift coefficient (b) Moment coefficient

Fig. 5. Time histories of lift and moment coefficient of a NACA 64A010 airfoil
M=0.796, Re=1.2E+07, α_0=0, α_1=1.02, k=0.404, x_p=0.25c

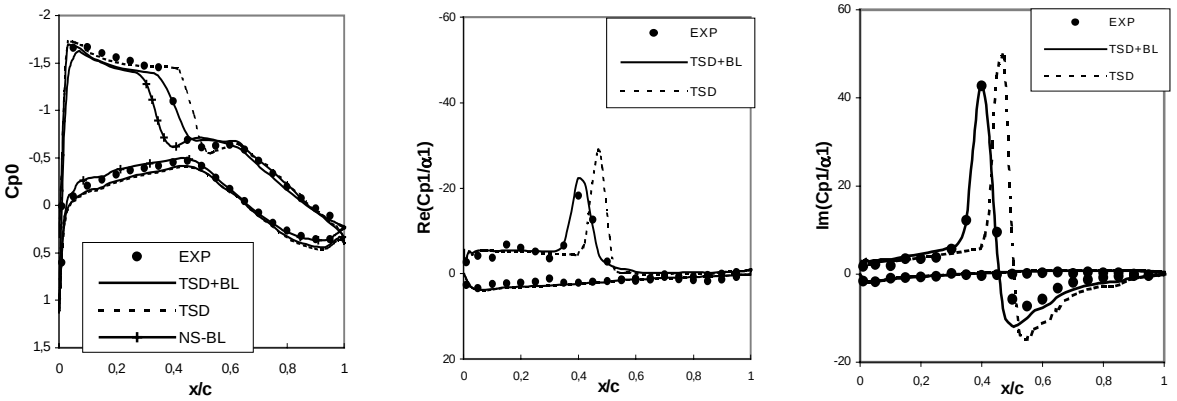

a) zero harmonic b) Real part of 1st harmonic c) Imaginary part of 1st harmonic

Fig. 6. Pressure Distribution of NLR 7301 airfoil at M=0.7, Re=2.14E+06, α_0 = 2.0, α_1=0.5, k=0.384, x_p=0.4c

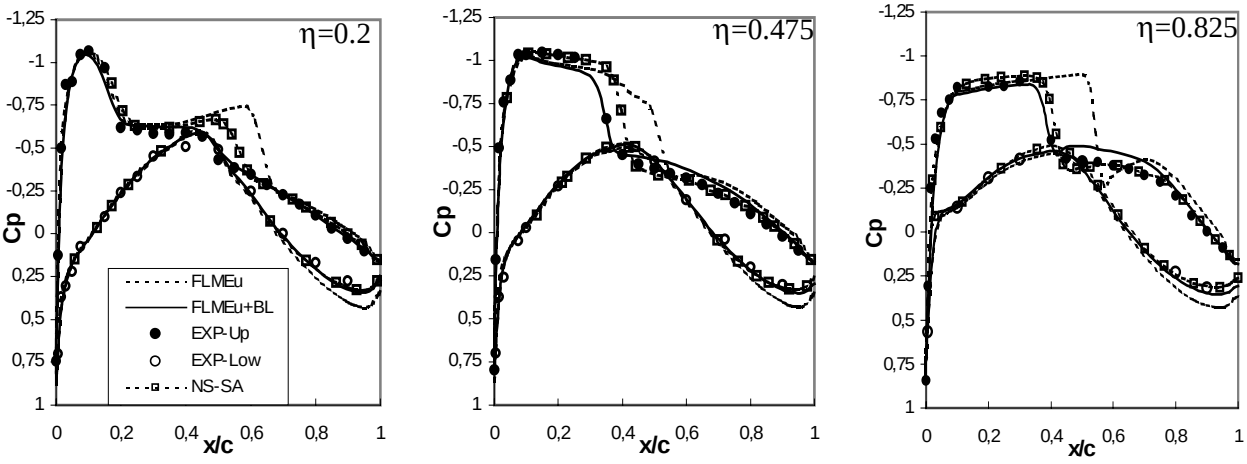

Fig. 7. Steady Pressure Distribution of LANN Wing, CT5 Case
M=0.82, Re=7.34E+06, α_0=0.6

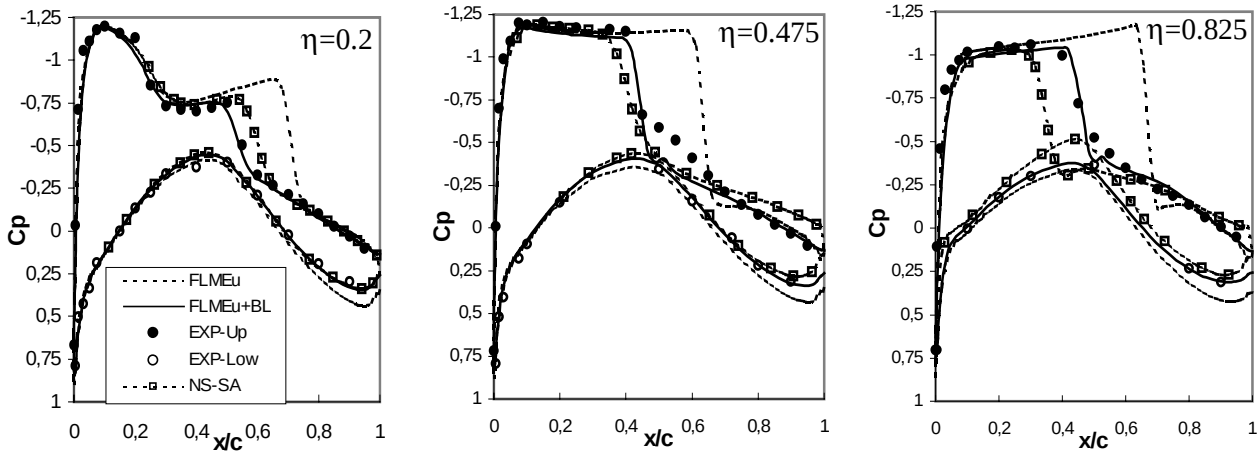

Fig. 8. Steady Pressure Distribution of LANN Wing, CT9 Case
M=0.82, Re=7.17E+06, α_0=2.2

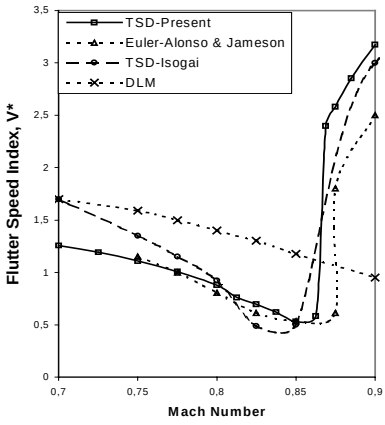

Fig.9. V^* v/s M
for Isogai model (NACA64A010)

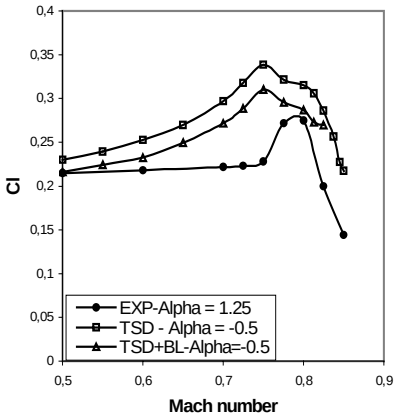

Fig.10. Cl v/s M
for DLR model (NLR 7301)

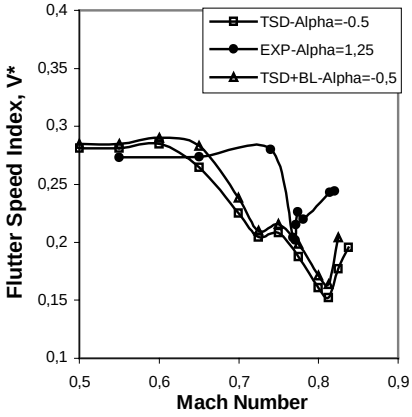

Fig. 11. V^* v/s M
for DLR model (NLR 7301)

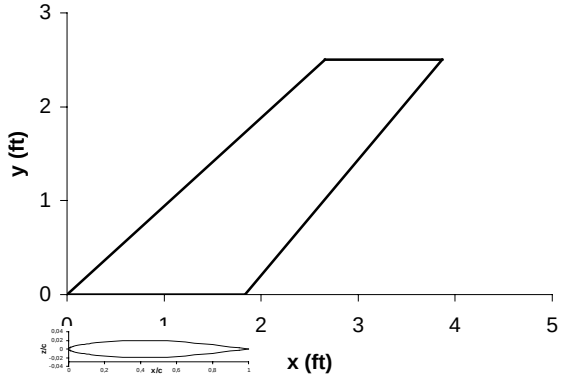

Fig. 12. AGARD Wing 445.6

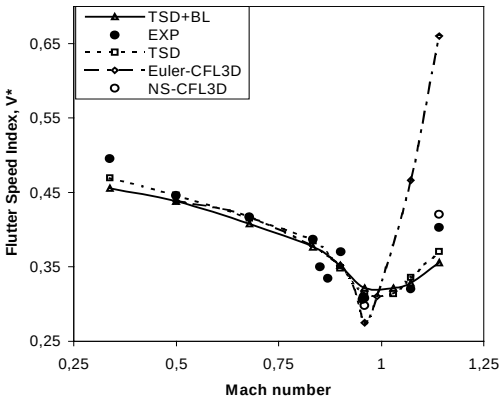

Fig.13. V^* v/s M of AGARD Wing 445.6